Fabrication and characterization of high-T/sub c/ SQUID magnetometer with damping resistance

著者	MATSUDA Mizushi, OTOWA T., MATSUURA T., KURIKI Shinya, KAWAGUCHI Y., TAKAHASHI K.
journal or publication title	IEEE transactions on applied superconductivity
volume	13
number	2
page range	853-856
year	2003-06
URL	http://hdl.handle.net/10258/207

doi: info:doi/10.1109/TASC.2003.814066

Fabrication and Characterization of High-T_c SQUID Magnetometer With Damping Resistance

M. Matsuda, T. Otowa, T. Matsuura, S. Kuriki, Y. Kawaguchi, and K. Takahashi

***Abstract*—Effects of damping resistance on current versus voltage (I-V) characteristics for high-T_c superconducting quantum interference devices (SQUIDs) were studied. In the transverse-type SQUID with coplanar strip lines, parasitic capacitance originating from the large dielectric constant of $SrTiO_3$ substrates can induce resonance structures on I-V curves and degrade the modulation voltage. In our simulations, it is shown that the modulation voltage is much improved by using damping resistance. However, the obtained experimental results for our SQUIDs with Au damping do not agree well with those in the simulations. The discrepancy is likely due to existence of the large contact resistance between Au and $YBa_2Cu_3O_{7-\delta}$ films.**

***Index Terms*—Damping resistance, modulation voltage, resonance phenomena, SQUIDs.**

I. Introduction

In fabricating grain boundary junctions, $SrTiO_3$ (STO) has been widely used as a substrate for $YBa_2Cu_3O_{7-\delta}$ (YBCO) film deposition, though it has large dielectric constant, $\varepsilon_r = 1930$ [1] at 77 K. This high permittivity was not thought to bring about serious problems in superconducting quantum interference devices (SQUIDs) where the frequency of Josephson oscillation is relatively low. However, for the practical SQUID with inductance formed by a pair of coplanar lines, the resonance phenomenon takes place as a result of the formation of standing electromagnetic waves within the STO between the strips. The resonance can induce some changes in the current-voltage (I-V) characteristics of the SQUID such as the occurrence of the crossover structure between the curves at $n\Phi_0$ and $(n+1/2)\Phi_0$. Here, Φ_0 is the flux quantum. The presence of this structure can degrade the modulation voltage, ΔV, of the SQUID. Especially for the transverse-type SQUID with a long hole parallel to the bicrystal line and junctions at each end of the hole, the resonance voltage, V_r, is calculated [1] in terms of ε_r, Φ_0, strip line length of l, velocity of light of c, and the number for flux quanta of n, using the following two relations:

$$V_r = \begin{cases} \frac{mc}{2l\sqrt{\frac{\varepsilon_r+1}{2}}}\Phi_0 & \text{for } n\Phi_0 \\ \frac{mc}{4l\sqrt{\frac{\varepsilon_r+1}{2}}}\Phi_0 & \text{for } \left(n+\frac{1}{2}\right)\Phi_0 \end{cases} \quad (1)$$

Manuscript received August 6, 2002.

M. Matsuda and T. Otowa are with Muroran Institute of Technology, Muroran, Hokkaido, Japan (e-mail: matsuda@mmm.muroran-it.ac.jp).

T. Matsuura was with Muroran Institute of Technology, Muroran, Hokkaido, Japan and is now with Fujitsu Ltd., Kawasaki, Kanagawa, Japan (e-mail: matsuura_t@jp.fujitsu.com).

S. Kuriki, Y. Kawaguchi, and K. Takahashi are with Research Institute for Electronic Science, Hokkaido University, Sapporo, Hokkaido, Japan (e-mail: sk@es.hokudai.ac.jp).

Digital Object Identifier 10.1109/TASC.2003.814066

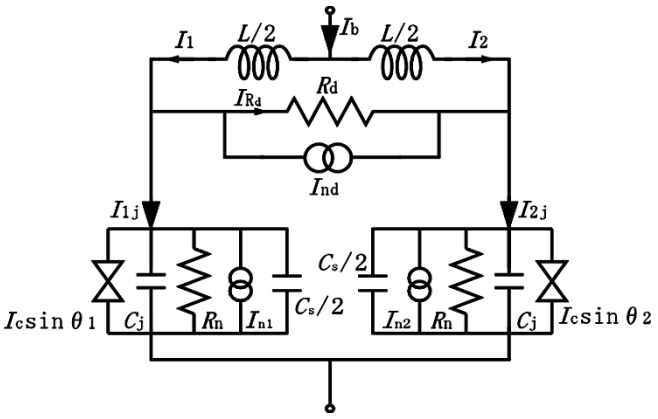

Fig. 1. An equivalent circuit of a transvers-type SQUID by lump components.

where, $m = 1, 3, 5, \ldots$. One of the solutions to avoid resonance and to improve ΔV is the use of $[LaAlO_3]_{0.3}[Sr(Al, Ta)O_3]_{0.7}$ (LSAT) substrates with low permittivity [2]. However, it is currently very difficult to purchase LSAT bicrystal substrates.

We studied the effect of the damping resistance that exists parallel to the inductance of the SQUID in a distributed manner, using both analytical and experimental methods. It has been already reported that degradation of ΔV due to large SQUID inductances can be recovered when the damping resistance, which is regarded as a lump component, is introduced [3]–[5]. In this paper, first, we show results of numerical simulations for the damping effect by a lump circuit model. Next, experimental results for YBCO SQUIDs with the Au damping resistance are shown. Finally, we discuss the effect of contact resistance between Au and YBCO by using results of analytical calculations by a distributed impedance circuit model.

II. Lump Model Simulation

In this model, inductance, capacitance, and resistance are regarded as the lump components in the equivalent circuit for the transverse-type SQUID shown in Fig. 1. Here, C_s represents a parasitic capacitance component between strip lines, and R_d is a damping resistance. I_n are noise currents with Gaussian random variables due to the thermal noise associated with the resistances. We derived the set of equations describing time-dependent behavior and obtained the dc voltage, V, of the SQUID as a function of bias current, I_b, by averaging the voltage of two junctions over time period which are long compared with the Josephson period [6]. Fig. 2 shows the simulated I-V characteristics of the SQUIDs with various values of damping resistance. Here, we used the normal resistance $R_n/2$ of 6 Ω, a critical current $2I_c$ of 32 μA, SQUID inductance L of 73 pH,

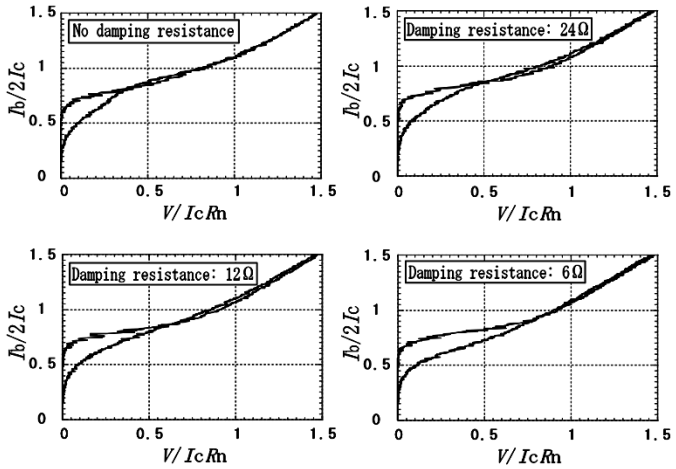

Fig. 2. Simulated I-V characteristics of SQUIDs with various values of damping resistance.

inductance parameter $\beta_L = 2LI_c/\Phi_0$ of 1.13, capacitance parameter $\beta_c = [2\pi I_c R_n^2(C_j + C_s/2)]/\Phi_0$ of 2.98, and temperature T of 77 K, from the experimental values. The current step occurs when the frequency of the Josephson current coincides with a resonance frequency of the L-$2C_j$-C_s circuit. Then, for the SQUID without damping, the voltage at which the current step occurs can be given by

$$V_r = \Phi_0 \sqrt{\frac{1}{2\pi^2 L(2C_j + C_s)}}. \tag{2}$$

For the SQUID with resistance, R_d, parallel to the inductance, L, the resonant current is damped depending on the value of R_d. It can be seen that a crossover point of the two I-V curves shifts to a higher voltage region with decreasing of R_d values. Even the relatively large damping resistance, R_d, of 24 Ω, which is two times larger than the junction resistance, R_n, is effective for the improvement of ΔV.

III. Experimental Results

The SQUID magnetometers are prepared from c-axis oriented YBCO films. A 150 nm thick film of YBCO and a 10–200 nm thick film of Au were deposited sequentially without breaking vacuum by a pulsed laser deposition on a 10 mm × 10 mm STO bicrystal substrate with a misorientation angle of 30°. They show a transition temperature of 89 K and a critical current density at 77 K exceeding 5×10^6 A/cm^2 except at the grain boundaries. Measured resistivity of our Au film at 77 K was around 1.2 $\mu\Omega \cdot$ cm. The films were patterned to form the magnetometer geometry illustrated in Fig. 3 by Ar ion beam etching and standard photolithography. The transverse-type SQUID has two parallel strips of 5 μm width and a long hole parallel to the bicrystal line. The hole length and width are 58-70 and 10 μm, respectively. The 1.5–2.5 μm wide bridges including grain boundary junctions are located at the both sides of the hole. Two separate pickup coils are connected to the right and left ends of the upper and lower strips in order to form the direct-coupled scheme. In this geometry, high coupling of

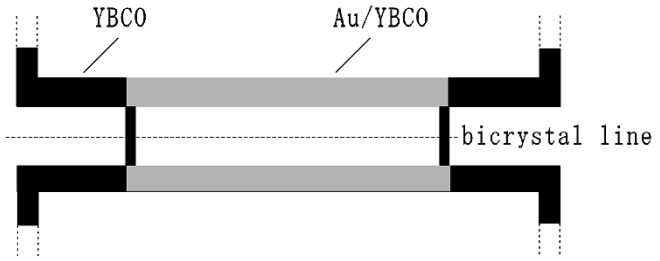

Fig. 3. Geometry of a transverse-type SQUID fabricated.

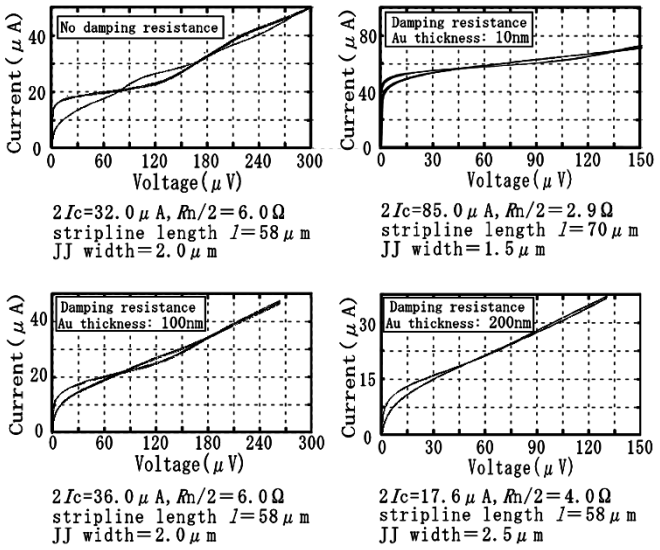

Fig. 4. I-V characteristics of fabricated SQUIDs without and with damping resistance for different Au film thickness.

more than 80% is obtained [7]. Au films left only on the YBCO strip lines by wet etching using KI solution act as the damping resistance. In this shape, a Au thickness of 10, 100, and 200 nm corresponds to the value of the damping resistance, R_d, of 27.1, 3.3, and 1.4 Ω, respectively.

Fig. 4 shows the I-V characteristics of fabricated SQUIDs without and with damping resistance for different Au film thicknesses. In the case of the SQUID without damping resistance, the curves exhibit multiple steps clearly due to the formation of higher modes standing electromagnetic waves. Observed voltages at the first ($m = 1$) steps for $n\Phi_0$ and $(n + 1/2)\Phi_0$ agree well with the calculated values for V_r of 172 and 86 μV by (1). For the SQUID with damping resistance, contrary to results of the lump model simulation, a significant shift of the crossover point was not observed throughout this region of Au thickness. Measured values of ΔV for each SQUID are listed in Table I. For comparison, the expected values for SQUIDs without damping resistance given by Enpuku *et al.* in [8]:

$$\Delta V_{cal} = \frac{4}{\pi} \frac{I_c R_n}{1 + \beta_L} \exp\left(\frac{-3.5\pi^2 k_B T L}{\Phi_0^2}\right) \tag{3}$$

are also shown in this Table. The ratio of ΔV to ΔV_{cal} is 0.4–0.7 and is independent of the value of the damping resistance. Hence we cannot confirm any suppression of the resonance phenomenon.

TABLE I
PARAMETERS OF THE SQUIDS OBTAINED

Damping resistance Au thickness (nm)	$IcRn(\mu V)$	β_L	$\Delta V(\mu V)$	$\Delta V_{cal}(\mu V)$	$\frac{\Delta V}{\Delta V_{cal}}$
0	220	1.27	44	63	0.70
10	243	3.53	18	32	0.56
100	190	1.13	41	61	0.67
200	70	0.62	12	30	0.41

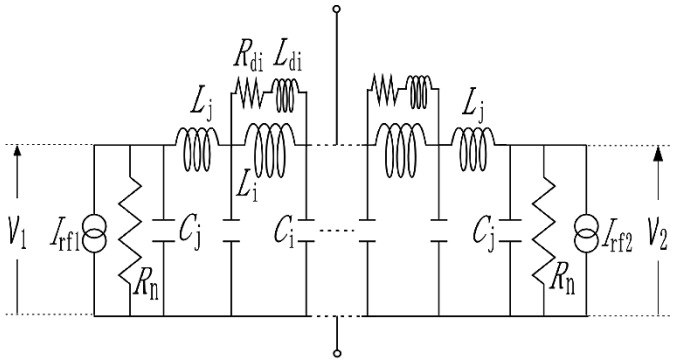

Fig. 5. An equivalent circuit of a transverse-type SQUID including the distributed impedance of coplanar strip lines.

IV. DISTRIBUTED IMPEDANCE MODEL ANALYSIS

Obtained experimental results for the SQUIDs with Au damping do not agree well with those in the lump model simulations. One of the possible reasons for the discrepancy is the existence of the inductance component for the Au damping resistor, and contact resistance between Au and YBCO films. Both of them were not taken into account in the simulation and could exist in a distributed manner. In our previous study [9], we showed that the I-V characteristics and their change with applied flux can be calculated analytically if the impedance function of the SQUID can be expressed with a four terminal network circuit.

Fig. 5 shows the equivalent circuit of the transverse-type SQUID including the distributed impedance of coplanar strip lines. Here, L_i and C_i represent an inductance and a capacitance per unit length for the strip lines, respectively. R_{di} and L_{di} are a damping resistance including contact resistance for Au/YBCO and an inductance component for Au damping layer per unit length, respectively. We assumed the contact resistance between Au and YBCO films deposited by in-situ process to be about $5 \times 10^{-9}\ \Omega \cdot \mathrm{cm}^2$ [10], [11]. The Josephson currents of junctions in the voltage states are simplified to a sinusoidally oscillating rf currents, on which the dc supercurrent is superimposed. The applied flux is expressed as a phase difference between the two rf currents. Time-dependent voltages across the junctions are determined from the interaction of rf currents after modification by the complex impedance between two junctions. Fig. 6 shows the calculated I-V curves of SQUIDs without and with damping resistance for different Au film thicknesses. Here, we assumed the strip line length of 58 μm. The other parameters are as followed; $R_n/2 = 6\ \Omega$, $2I_c = 32\ \mu$A, $L = 73$ pH,

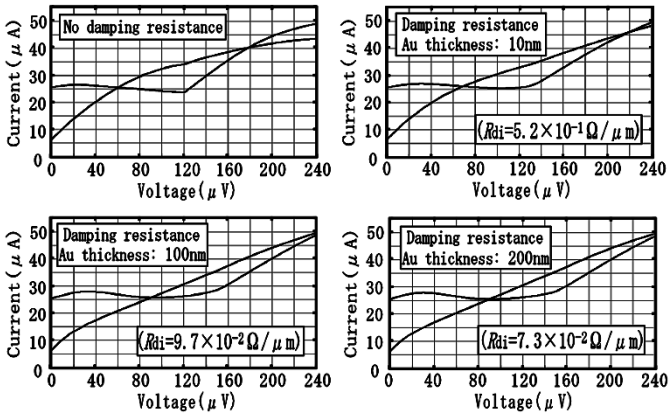

Fig. 6. Calculated I-V curves of SQUIDs without and with damping resistance for different Au film thickness.

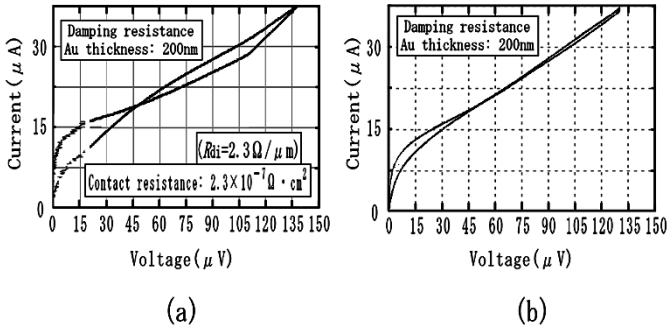

Fig. 7. Calculated (a) and measured (b) I-V characteristics of a SQUID with 200 nm thick Au damping resistance. Curves in (a) at low voltage region are given by lump model simulations.

$L_i = 1.12$ pH/μm, $C_i = 11.26$ fF/μm, $L_{di} = 0.43$ pH/μm, and $T = 77$ K. It is shown that multiple crossover structure on the I-V characteristics are expressed by the distributed impedance model. Especially for the SQUID without damping, calculated curves can be well fitted to the experimental results shown in Fig. 4 except for the very low voltage region. The main cause of the deviation in this region is the strong nonsinusoidal behavior of the Josephson oscillation at low voltages, which is neglected in the sinusoidal approximation in the present analytical calculation. With the decrease of the damping resistance values, we can also see considerable shifts of the crossover point to higher voltages as shown in Fig. 6.

If we introduce an extremely larger value for R_{di} than the first assumption of $5 \times 10^{-9}\ \Omega \cdot \mathrm{cm}^2$, the calculated results of the analysis will drastically change. The larger R_{di} by two orders of magnitude could weaken the damping effect and explain the experimental results. Whereas the large L_{di} works in the similar way, it is not likely that the L_{di} value is larger by two orders of magnitude than that estimated from the geometry. Fig. 7(a) shows the calculated I-V curves for a SQUID with contact resistance of $2.3 \times 10^{-7}\ \Omega \cdot \mathrm{cm}^2$. The other parameters are as follows; strip line length of 58 μm, Au film thickness of 200 nm, $R_n/2 = 4\ \Omega$, $2I_c = 17.6\ \mu$A, $L = 70$ pH, $L_i = 1.12$ pH/μm, $C_i = 13.36$ fF/μm, $L_{di} = 0.43$ pH/μm, and $T = 77$ K. At low voltage region near the supercurrent, I-V curves are replaced by the results given by a lump model simulation. The

measured results for a SQUID with a 200 nm thick Au damping resistance are also shown in Fig. 7(b) for comparison. Characteristics obtained by the analytical calculation agree reasonably with the experimental results. The contact resistances between Au/YBCO films deposited by in-situ and ex-situ processes were reported to be about $10^{-9}\ \Omega\cdot\mathrm{cm}^2$ and $10^{-5}\ \Omega\cdot\mathrm{cm}^2$, respectively [10], [11]. Our assumption of $2.3\times10^{-7}\Omega\cdot\mathrm{cm}^2$ lies between two extremes. Up to now, we can only confirm that the contact resistance in our Au/YBCO film interface is at least lower than $3\times10^{-5}\ \Omega\cdot\mathrm{cm}^2$. It seems to be important to evaluate the contact resistance value precisely and reduce it.

V. Conclusion

We studied the effect of the damping resistance existing parallel to the inductance of the SQUID in a distributed manner, analytically and experimentally. Characteristics obtained by the analysis calculation agreed reasonably with the experimental results when we took account of the considerably large contact resistance around $10^{-7}\ \Omega\cdot\mathrm{cm}^2$ between Au and YBCO films.

References

[1] L. P. Lee, J. Longo, V. Vinetskiy, and R. Cantor, "Low-noise $YBa_2Cu_3O_{7-\delta}$ direct-current superconducting quantum interference device magnetometer with direct signal injection," *Appl. Phys. Lett.*, vol. 66, pp. 1539–1541, March 1995.

[2] M. Matsuda, S. Ono, K. Kato, K. Yokosawa, H. Oyama, and S. Kuriki, "High-T_c SQUIDs on bicrystal substrate with low permittivity," *Extended Abstracts of 7th International Superconducting Electronics Conference*, pp. 137–139, 1999.

[3] K. Enpuku, H. Doi, G. Tokita, and T. Maruo, "Modulation voltage of high-T_c superconducting quantum interference device with damping resistance," *Jpn. J. Appl. Phys.*, vol. 33, pp. L722–L725, May 1994.

[4] D. Suzuki, S. Kuriki, and M. Matsuda, "Effect of damping resistance on the modulation voltage of large-inductance high-T_c superconducting quantum interference devices," *Jpn. J. Appl. Phys.*, vol. 34, pp. L1641–L1643, Dec. 1995.

[5] F. Kahalmann, W. E. Booji, M. G. Blamire, P. E. McBrien, and E. J. Tarte, "Performance of high-T_c SQUID magnetometers with resistively shunted inductances compared to "unshunted" device," *IEEE Trans. Applied Superconductivity*, vol. 11, pp. 916–919, March 2001.

[6] M. Matsuda, M. Kubo, S. Kuriki, K. Masuzawa, and R. S. Ahmad, "Analysis of high-T_c SQUIDs with large capacitance components," in *Advances in Superconductivity IX*: Springer-Verlag, 1997, vol. 2, pp. 1221–1224.

[7] E. Maruyama, S. Kuriki, K. Yokosawa, and R. S. Ahmad, "Flux coupling in the direct-coupled high-T_c superconducting quantum interference devices," *Jpn. J. Appl. Phys.*, vol. 37, pp. L722–L724, June 1998.

[8] K. Enpuku, G. Tokita, T. Maruo, and T. Minotani, "Parameter dependencies of characteristics of high-T_c superconducting quantum interference device," *J. Appl. Phys.*, vol. 78, pp. 3498–3503, Sep. 1995.

[9] E. Maruyama, S. Kuriki, Y. Kurisu, and M. Matsuda, "Analytical approach to calculate the flux dependent current-voltage characteristics of dc superconducting quantum interference devices," *J. Appl. Phys.*, vol. 83, pp. 6166–6171, June 1998.

[10] J. Du, S. K. H. Lam, and D. L. Tilbrook, "Metallization and interconnections of HTS YBCO thin film devices and circuits," *Supercond. Sci. Technol.*, vol. 14, pp. 820–825, 2001.

[11] K. Mizushima, "Metal contact characteristics," *OYO BUTURI*, vol. 60, pp. 486–487, 1991.